Journal of Computational Physics 308 (2016) 421–437

Contents lists available at ScienceDirect

Journal of Computational Physics

www.elsevier.com/locate/jcp

Steepest descent ballistic deposition of complex shaped particles

Nikola Topic, Thorsten Pöschel *

Institute for Multiscale Simulation, Friedrich-Alexander-Universität, Erlangen, Germany

ARTICLE INFO

Article history:
Received 24 May 2015
Received in revised form 22 December 2015
Accepted 26 December 2015
Available online 30 December 2015

Keywords:
Steepest descent ballistic deposition
Non-spherical particles
Complex shaped particles
Event-driven algorithm

ABSTRACT

We present an efficient event-driven algorithm for sequential ballistic deposition of complex-shaped rigid particles. Each of the particles is constructed from hard spheres (typically 5 . . . 1000) of variable radii. The sizes and relative positions of the spheres may mutually overlap and can be chosen such that the surface of the resulting particle appears relatively smooth. In the sequential deposition process, by performing steps of rolling and linear motion, the particles move along the steepest descent in a landscape formed by the boundaries and previously deposited particles. The computer time for the simulation of a deposition process depends on the total number of spheres but only weakly on the sizes and shapes of the particles. The proposed algorithm generalizes the Visscher–Bolsterli algorithm [1] which is frequently used for packing of spheres, to non-spherical particles. The proposed event-driven algorithm allows simulations of multi-million particle systems using desktop computers.

1. Introduction

The numerical description of sedimentation processes of particles on a flat or curved surface under the action of gravity or another external force, is essential for the understanding of a wide range of phenomena. Therefore, efficient algorithms for sedimentation processes are needed. Among others, processes such as filtration, e.g. [2], various types of size segregation phenomena [3–5] and the structure of certain types of packing have been investigated, e.g. [1,6–10]. While the latter application is certainly the most important evidenced by an enormous body of literature, we wish to point out, however, that the general problem of packing, that is, arranging objects in a confined space, frequently aiming to highest density, is related but not identical to the problem of sedimentation. Similarly, the corresponding simulation methods, referred to as *packing algorithms* cover a much wider field than simulation of sedimentation, see comprehensive reviews on packing, e.g. [11,12] and packing algorithms, e.g. [13–15].

Early literature describes mainly sedimentation algorithms for monodisperse or polydisperse spheres due to simplicity of contact detection for spheres. However, obviously particle shape has an important effect on the packing structure and, thus, the physical properties of sediments, therefore, there is a need for simulations of non-spherical particles. Sedimentation of non-spherical particles was investigated by several authors using different particle models such as ellipsoids [16,17], spherocylinders [18,19], polygons (in 2d) [20,21] or polyhedrons [22] representing sharp edged particles and pixel or voxel descriptions of the particles [23], for a review see [15]. Of particular interest for the simulation of non-spherical particles

* Corresponding author.
E-mail address: thorsten.poeschel@fau.de (T. Pöschel).

http://dx.doi.org/10.1016/j.jcp.2015.12.052
0021-9991/

are *multisphere models*, e.g. [24–27], where each particle is represented by a set of monodisperse or polydisperse spheres. Similarly as for spheres, contacts of such particles can be easily detected. On the other hand, by appropriately choosing the radii and relative positions of the constituting spheres, a multisphere particle can approximate any desired shape to arbitrary accuracy, provided the set of spheres is large enough. Therefore, the multisphere model compromises between numerical efficiency and realistic particle shape.

The dynamics of non-spherical particles in sedimentation processes follows Newtonian mechanics which is approximately solved numerically by Molecular Dynamics, e.g. [17,28], but also other techniques have been applied, such as Monte Carlo methods [23,16,18,29] and others [15]. A class of simulation methods particularly adopted to the problem of sedimentation of particles in gravity is referred to as *drop and roll algorithms* or *steepest descent ballistic deposition algorithms* (SDBD). There are three paradigms behind these algorithms going back to the pioneering work by Vold [30]: (a) the particles are deposited sequentially, one after the other; (b) the particles obey overdamped dynamics, along the steepest descent with respect to gravity in the landscape shaped by previously deposited particles and the container walls until the particle reaches a (meta-) stable position where the particle is deposited; (c) once deposited, the particles do not change their position. This algorithm was first described by Visscher and Bolsterli [1], and is discussed in detail in [31–33].

Following the path of steepest descent implies a sequence of motion of different type: the particle may (i) fall vertically, (ii) roll in contact with one other particle or (iii) roll in contact with two other particles. Changes of the type of motion correspond to changes of the number of contacts of the particle considered. The great advantage of SDBD is that its dynamics may be described as a sequence of discrete events [34], where the events correspond to the change of the type of motion. Therefore, SDBD can be simulated by event-driven algorithms, which are by orders of magnitude faster than by integrating Newton's equation of motion in Molecular Dynamics allowing for simulations of large systems, needed for statistical analysis of packings (see [8] for a simulation of up to 2.5×10^7). There exist different strategies to optimize the efficiency of SDBD-algorithms [33].

Unlike Molecular Dynamics, SDBD is not a universal algorithm for the dynamics of particle systems as it neglects the inertia of particles (see, e.g. [8]). Nevertheless, it has been successfully applied to a wide range of problems in physics and engineering, such as microstructure modeling of fuel cells [35], charge stabilized colloids [36], packings in pebble bed reactors [37], nano-structured materials [14], metallic glasses [38], problems in additive manufacturing [39], processing of minerals [40], microstructure of ash deposits [41,42], sintering [43], microstructure of reaction-sintered ceramics [44], porous media [45,46] and many others.

2. Steepest descent ballistic deposition of aggregates

By now, the literature covers only SDBD algorithms for mono- and polydisperse spheres and simple non-spherical particles such as ellipsoids or rods [47,48]. Realistic particles are, however, frequently of more complex shape, therefore, in this papers we describe an efficient and robust SDBD algorithm for the sedimentation of complex-shaped particles. Following the basic idea of multisphere particles frequently used in Molecular Dynamics simulations, the particles considered here are rigid aggregates of polydisperse spheres arranged in overlapping or non-overlapping relative positions. This algorithm presented here was applied in numerical investigations of the packing properties in agglomerates of nano-powders [10] (for a 2d version see [9]).

Fig. 1 shows examples of complex shaped particles also termed aggregates in the following. By choosing appropriate radii and relative positions (overlapping or non-overlapping) of the constituting spheres, different shapes can be modeled. Fig. 1(a) shows a rod-shaped particle consisting of 11 equal overlapping spheres, Fig. 1(b) shows a particle composed of 4 equal rods having in total 17 overlapping spheres, while Fig. 1(c) shows an agglomerate of 790 non-overlapping spheres as used in a simulation of packings of nano-particles [10]. Using multi-sphere method particle shape can be represented with high precision, e.g. Fig. 1(d) shows a particle composed of 1785 spheres, Fig. 1(e) shows a particle with 2520 spheres, and finally the particle in Fig. 1(f) has 6241 spheres.

While in most practical applications complex particles are modeled as aggregates of overlapping polydisperse spheres, in the following illustrations for the sake of clearness, we will sketch aggregates of non-overlapping equal sized spheres. The presented algorithm is, however, not restricted to this case.

The algorithm for steepest descent ballistic deposition of sphere aggregates presented here preserves the basic idea introduced by Visscher and Bolsterli [1] for simulations of the deposition of spheres: Particles are sequentially dropped and follow the path of the steepest descent on the surface of the landscape formed by the system boundary and by previously deposited particles. Once found a stable position in a local minimum, the particle is immobilized. Owed to the non-spherical shape of the particles, the motion along the steepest descent path is modified. First, it is not the center of a sphere which follows the steepest descent but the center of mass of the agglomerate and second, following the steepest descent, the dropped particle adopts slightly different modes of motion than described in [1], illustrated in Fig. 2. When not in contact with any other particle nor the container wall, the agglomerate moves vertically downwards, thus, following the steepest descent, Fig. 2(a). When having one contact, that is, one of the spheres constituting the aggregate is in contact with one sphere of the previously sedimented material or the wall, the aggregate rotates around an axis which is specified by the center of the immobile sphere and by the condition that the center of mass of the aggregate follows the steepest descent, see Fig. 2(b). When having two contacts, Fig. 2(c), the aggregate rotates around an axis specified by the centers of the

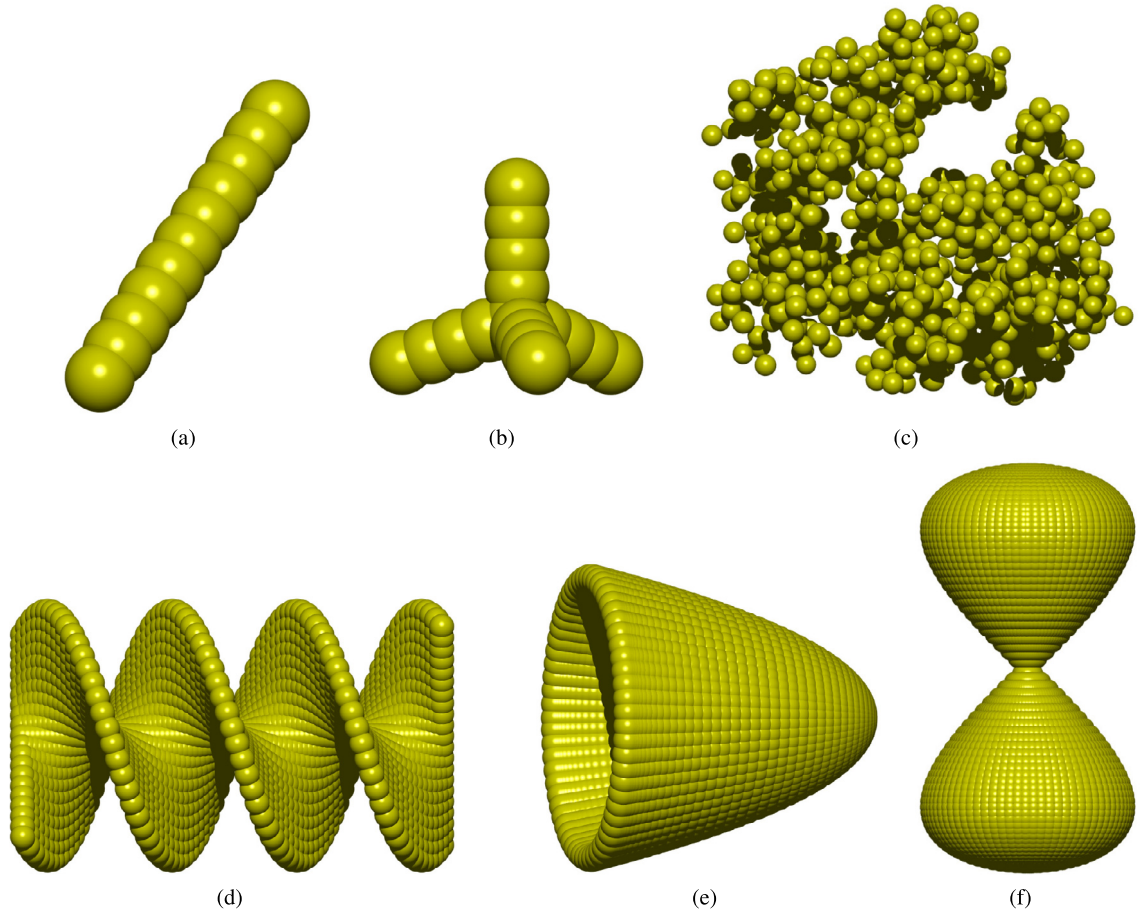

Fig. 1. Examples of complex shaped particles. (a) Rod. (b) Particle composed of 4 equal rods. (c) Fractal agglomerate (see [10]). (d)–(f) Particles composed of large number of spheres.

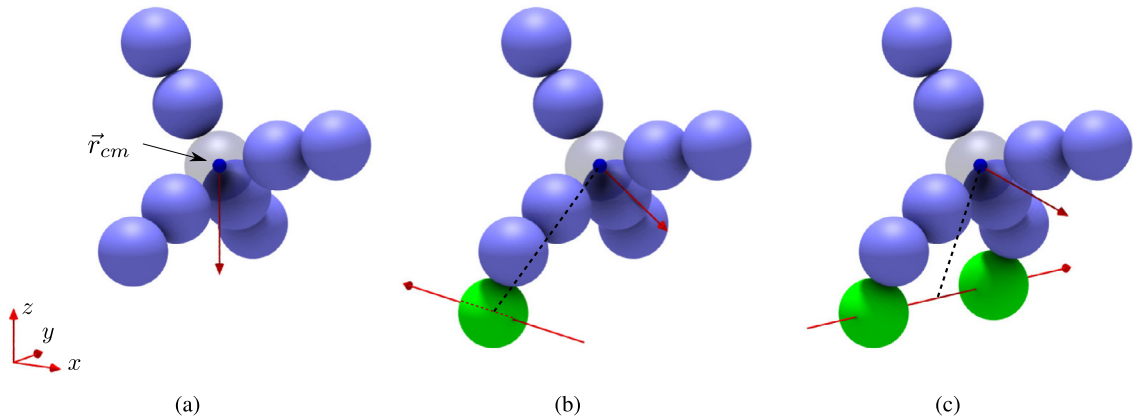

Fig. 2. Types of motion of an aggregate following the steepest descent. (a) Vertical translation of the center of mass. (b) Rotation of the aggregate when in contact with one immobile sphere. (c) When in contact with two immobile spheres, rotation of the aggregate around the axis defined by the immobile spheres. The center of mass, $\vec{r}_{\mathrm{cm}}$, is indicated by a small blue sphere. Red arrows show the direction of motion of the center of mass and the rotation axes in (b) and (c). The black dashed lines in (b) and (c) are normal to the rotation axes, and connect the rotation axes with the centers of mass. In all cases, the vertical position of the center of mass decays. (For interpretation of the references to color in this figure legend, the reader is referred to the web version of this article.)

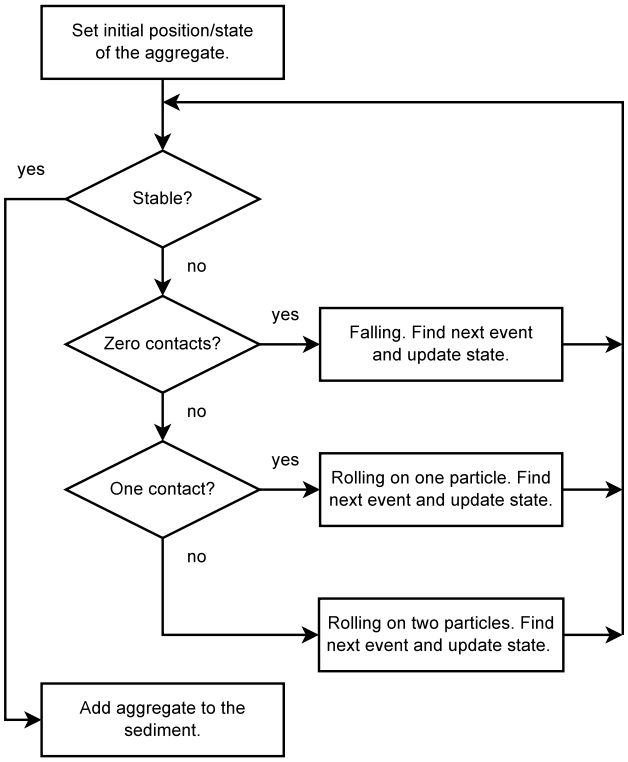

Fig. 3. Flow diagram for the sedimentation of an aggregate. During the sedimentation the aggregate can follow a complex trajectory with many events where it changes its contacts.

involved two immobile particles and the sense of the rotation is such that the vertical position of the center of mass decreases.

The path of the aggregate from its starting position to the place where it finds its local minimum in contact with 3 immobile particles or the system wall, is described by a sequence of movements of type (i), (ii) and (iii). Transitions between these types of motion correspond to changes of the contacts. These changes, in turn, are enforced by the condition that the aggregate shall always follow the path of steepest descent.

The described model defines the path of the aggregate uniquely. Moreover, for any given situation, specified by the current position of the aggregate and the previously deposited particles we could analytically compute the position of the aggregate at the time when the next change of the contacts occurs, that is, when any of the existing contacts opens or a new contact is established. Therefore, the model for steepest descent ballistic deposition of aggregates may be formulated by an event-driven algorithm where the events are given by the changes of the number of contacts of the aggregate. Event-driven simulations where in each step the aggregates motion from one event to the next is computed, may be by orders of magnitude more efficient than time-step controlled algorithms such as Molecular Dynamics. The crucial part of the algorithm is to find the next event starting from a current configuration, characterized by a certain number of contacts, see cases (i)–(iii). In the next section, we will consider each of the cases (i)–(iii) and explain how the next event is found. The flow diagram for the sedimentation of an aggregate is shown in Fig. 3.

3. Event-driven algorithm

We start from a given configuration defined by the structure of the complex particles, specified by the radii and current positions of the constituting spheres, the structure of the landscape, specified by the radii and positions of the spheres belonging to previously sedimented aggregates and the system boundaries which may be rigid walls or periodic in horizontal directions. For an event-driven algorithm, then we need to identify the next event, characterized by a change in the number of contacts and the position of the aggregate at the time of the event. In this section we will consider these questions for each of the types of motion (i)–(iii) specified above.

As for any event-driven algorithm a list of potential events must be compiled, for current state of the aggregate, in order to find the next event to be executed. The event which occurs next is the one for which the aggregate's center of mass travels the shortest distance in vertical direction starting from the current position. Starting from a certain configuration, variety of potential events may exist which are all added to the same list of potential events.

3.1. Case (i) – zero contacts

When the particle has zero contacts, it translates downward until one of its spheres either contacts one of the immobile spheres or the ground. Consider first sphere-sphere contacts. Possible candidates for the contact (ij) where i indicates a sphere from the aggregate of radius R_i^a at position $\vec{r}_i^{\,a} = \left(x_i^a, y_i^a, z_i^a\right)$ and j indicates an immobile sphere of radius R_j^s at position $\vec{r}_j^{\,s} = \left(x_j^s, y_j^s, z_j^s\right)$ satisfy the condition

$$\left(\Delta_{ij}^{xy}\right)^2 \equiv \left(R_i^a + R_j^s\right)^2 - \left(x_i^a - x_j^s\right)^2 - \left(y_i^a - y_j^s\right)^2 > 0\,, \tag{1}$$

where $\Delta_{ij}^{xy} \geq 0$. Out of these candidates, the pair which corresponds to the smallest positive value

$$\Delta_{ij}^{z} \equiv z_i^a - z_j^s - \Delta_{ij}^{xy} \tag{2}$$

will establish the next sphere-sphere contact. Correspondingly the aggregate, that is, all spheres constituting the aggregate are translated by

$$\vec{\Delta}^{sp} \equiv \begin{pmatrix} 0 \\ 0 \\ -\Delta_{ij}^{z} \end{pmatrix} \tag{3}$$

The case that more than one pair ij corresponds to the same numerical value Δ^z are discussed in Sec. 4.3. There exist various efficient methods to restrict the set of candidates (ij) which shall not be discussed here in detail. In our implementation, we sort the spheres of the aggregate with respect to their vertical coordinate, z_i^a, and start with the lowest sphere. The set of spheres of the sediment, j, to be investigated is restricted by means of a lattice in the xy plane where each lattice site contains the spheres located in this site. Only spheres j from lattice sites which comply with the condition Eq. (1) are possible candidates. The sediment particles in each lattice site are also sorted with respect to their vertical coordinate, z_j^s, and we start the search with the highest particle. As soon as a contact partner j is found for a certain i, we continue the search with the next possible site. Since the particles in the sediment are immobile, the computational costs of sorting are negligible although the total number of particles in the sediment may be large. Further acceleration is achieved by exploiting the fact that once a candidate pair (ij) is found only pairs (mn) with $\Delta_{mn}^z < \Delta_{ij}^z$ need to be considered.

Contacts of spheres of the aggregate with the system boundaries depend on the geometric shape of the walls. If there are only a bottom wall and vertical side walls or periodic horizontal boundary conditions, the contact is established through the particle i for which

$$\Delta_i^z \equiv z_i^a - z^w - R_i^a \tag{4}$$

adopts its minimum, where z^w is the vertical position of the bottom wall. In case of a sphere-wall contact, all spheres belonging to the aggregate are translated by

$$\vec{\Delta}^{w} \equiv \begin{pmatrix} 0 \\ 0 \\ -\Delta_i^z \end{pmatrix} \tag{5}$$

The generalization to other geometric shapes of the system boundary is straightforward.

Whether in case of the motion corresponding to zero contacts the subsequent event is a sphere-sphere or a sphere-wall contact depends on $\Delta_{ij}^z - \Delta_i^z$ where both quantities are meant to be of smallest value among all candidates i and j. The result of this type of motion will be either a wall contact, where the particle is immobilized or a position of the aggregate of type (ii) where it has one contact.

3.2. Case (ii) – one contact

3.2.1. Types of events

When an aggregate is in contact with one sphere of the sediment, 4 different events can result:

(a) the aggregate contacts a second sphere of the sediment
(b) the aggregate loses the contact
(c) the aggregate rotates until its center of mass is below the contact point at the same vertical coordinates
(d) the aggregate contacts the wall

Fig. 4 illustrates these cases (except of (d)) which shall be discussed in detail in the following subsections.

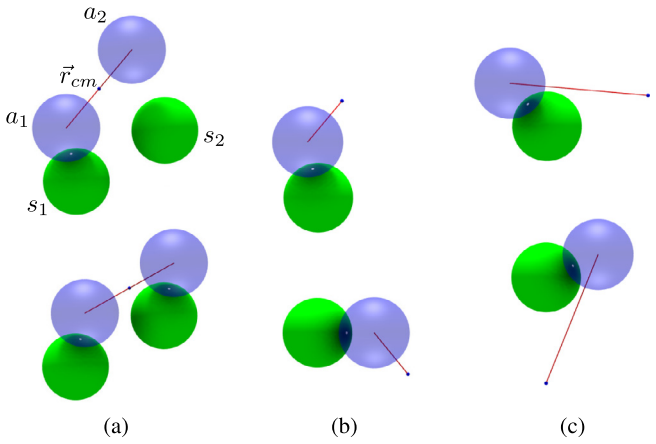

Fig. 4. Possible events resulting when the aggregate is in contact with one sphere of the sediment. Only spheres of the aggregate and the sediment which are involved in the contact are drawn. Spheres belonging to the aggregate (sediment) are drawn in blue (green). Initial situations are sketched in the upper part of the figure, final position in the lower part. Small blue spheres indicate the center of mass of the aggregate in its initial position. (a) The sediment rotates around s_1 until the second contact ($a_2 s_2$) is established. (b) The aggregate rotates until both spheres are at the same vertical position, there it loses contact. (c) The aggregate rotates until its center of mass is below the point of rotation at the same vertical coordinates. There the aggregate assumes its stable position. (For interpretation of the references to color in this figure legend, the reader is referred to the web version of this article.)

3.2.2. Event (a) – second contact

We consider the case when the aggregate is in contact with one sphere of the sediment and contacts a second one, Fig. 4(a). Let us first assume that initially sphere a_1 of the aggregate at position $\vec{r}_1^{\,a}$ is in contact with sphere s_1 of the sediment at position $\vec{r}_1^{\,s}$ and compute the positions of the aggregate when the contact of another pair of spheres, (a_2, s_2) is established. After that we will discuss the conditions under which one of these solutions corresponds to the subsequent event.

When following the steepest descent, the unit vector of the axis of rotation is parallel to the horizontal plane and determined by the position of particle s_1 and the center of mass of the aggregate, $\vec{r}_{\mathrm{cm}}$,

$$\vec{n} = \frac{\vec{e}_z \times \left(\vec{r}_{\mathrm{cm}} - \vec{r}_1^{\,s}\right)}{\left|\vec{e}_z \times \left(\vec{r}_{\mathrm{cm}} - \vec{r}_1^{\,s}\right)\right|}\,, \tag{6}$$

where $\vec{e}_z$ is the vertical unit vector. Possible positions $\vec{\varrho}_2^{\,a}$ of the particle a_2 due to this rotation are described by

$$\left|\vec{\varrho}_2^{\,a} - \vec{r}_1^{\,s}\right| = \left|\vec{r}_2^{\,a} - \vec{r}_1^{\,s}\right| \tag{7}$$

$$\left(\vec{\varrho}_2^{\,a} - \vec{r}_1^{\,s}\right)\vec{n} = \left(\vec{r}_2^{\,a} - \vec{r}_1^{\,s}\right)\cdot\vec{n}\,. \tag{8}$$

Equation (7) assures that the distance between the aggregate sphere a_2 and the center of rotation s_1 is invariant during the rotation and Eq. (8) assures that the direction of the rotation is $\vec{n}$. Solving Eqs. (7) and (8) together with the contact condition,

$$\left|\vec{\varrho}_2^{\,a} - \vec{r}_2^{\,s}\right| = R_2^a + R_2^s\,, \tag{9}$$

we obtain the position $\vec{\varrho}_2^{\,a}$ of the sphere a_2 at the instant of the contact, provided the system of equations has real solutions. In order to solve the system of equations (7)–(9) we consider the coordinate system with origin given by the projection of the point $\vec{r}_2^{\,a}$ onto the rotation axis $\vec{n}$,

$$\vec{O}\,' = \vec{r}_1^{\,s} + \left[\vec{n}\cdot\left(\vec{r}_2^{\,a} - \vec{r}_1^{\,s}\right)\right]\vec{n}, \tag{10}$$

and with the axes unit vectors

$$\vec{e}_x' = \frac{\vec{r}_2^{\,s} - \vec{r}_1^{\,s} - \left[\left(\vec{r}_2^{\,s} - \vec{r}_1^{\,s}\right)\cdot\vec{n}\right]\vec{n}}{\left|\vec{r}_2^{\,s} - \vec{r}_1^{\,s} - \left[\left(\vec{r}_2^{\,s} - \vec{r}_1^{\,s}\right)\cdot\vec{n}\right]\vec{n}\right|}\,; \qquad \vec{e}_y' = \vec{n}\times\vec{e}_x'\,; \qquad \vec{e}_z' = \vec{n}\,, \tag{11}$$

such that $\vec{e}_x'$ is the normalized vector pointing from the projection of $\vec{r}_2^{\,s}$ onto the axis of rotation $\vec{n}$ to $\vec{r}_2^{\,s}$, see Fig. 5. Note that the denominator of $\vec{e}_x'$ vanishes for the case when the sphere s_2 lies on the axis of rotation $\vec{n}$ which renders $\vec{e}_x'$ and $\vec{e}_y'$ undefined. This case which has to be accounted for in the algorithm is uncritical since then $\left|\vec{\varrho}_2^{\,a} - \vec{r}_2^{\,s}\right|$ is not affected by any rotation, that is, there is no contact (a_2, s_2).

Using the new coordinate system, the contact problem (7)–(9) reduces to computing the intersection points of two circles in the $x' - y'$ plane, see Fig. 5. One circle is of radius $R_1^c \equiv \left|\vec{r}_2^{\,a} - \vec{O}\,'\right|$ located at $\vec{r}_1^{\,c} \equiv \vec{O}\,'$ and the second circle is given by

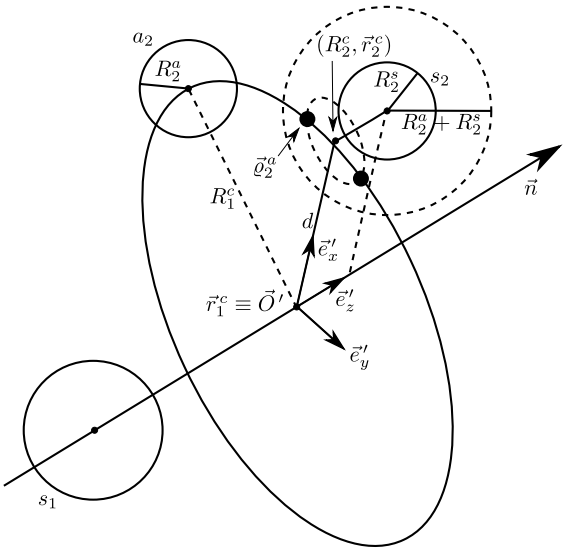

Fig. 5. Illustration of the coordinate system $\left(\vec{O}', \vec{e}_x', \vec{e}_y', \vec{e}_z'\right)$, together with relevant variables. Two black discs belonging to the circle $(R_2^c, \vec{r}_2^{\,c})$ indicate positions of the center of sphere a_2, when spheres a_2 and s_2 are in contact.

the section of a sphere at $\vec{r}_2^{\,s}$ of radius $R_2^s + R_2^a$ and the $x' - y'$ plane. Represented in the $x' - y'$ system, the second circle is located at $(d, 0)$ where d is the distance of the center of sphere s_2 from the axis $\vec{n}$. The radius of the second circle is

$$R_2^c \equiv \sqrt{\left(R_2^s + R_2^a\right)^2 - \left[\vec{n} \cdot \left(\vec{r}_2^{\,s} - \vec{O}'\right)\right]^2}, \tag{12}$$

where $\left|\vec{n} \cdot \left(\vec{r}_2^{\,s} - \vec{O}'\right)\right|$ is the distance of the center of sphere s_2 from the $x' - y'$ plane. The sign of the argument of the root in Eq. (12) determines whether contact of the pair $(a_2 s_2)$ is possible upon rotation of the aggregate. In case of a positive sign, we have two intersection points of the circles $\left(R_1^c, \vec{r}_1^{\,c}\right)$ and $\left(R_2^c, \vec{r}_2^{\,c}\right)$. Those two points are solutions of the system of equations (7)–(9).

We note that this solution is valid for any rotation axis $\vec{n}$, not just the ones parallel to horizontal.

Once the solution of the system is known, then it is necessary to rotate the whole aggregate. We avoided using rotation angle φ of the aggregate as its calculation would involve inverting trigonometric functions. Instead we calculate the pair of values $(\cos\varphi, \sin\varphi)$ since it can be obtained in a straightforward way from products of the relevant vectors, and contains the complete information about the rotation, i.e. a unique rotation angle corresponds to this pair. We obtain:

$$\cos\varphi = \frac{\left(\vec{\varrho}_2^{\,a} - \vec{O}'\right) \cdot \left(\vec{r}_2^{\,a} - \vec{O}'\right)}{\left|\vec{\varrho}_2^{\,a} - \vec{O}'\right| \left|\vec{r}_2^{\,a} - \vec{O}'\right|} \tag{13}$$

$$\sin\varphi = \frac{\left|\left(\vec{\varrho}_2^{\,a} - \vec{O}'\right) \times \left(\vec{r}_2^{\,a} - \vec{O}'\right)\right|}{\left|\vec{\varrho}_2^{\,a} - \vec{O}'\right| \left|\vec{r}_2^{\,a} - \vec{O}'\right|} \tag{14}$$

since $\left(\vec{\varrho}_2^{\,a} - \vec{O}'\right)$ and $\left(\vec{r}_2^{\,a} - \vec{O}'\right)$ are orthogonal to the rotation axis. The new position $\vec{\varrho}_i^{\,a}$ of any aggregate sphere i after the rotation by angle φ is:

$$\vec{\varrho}_i^{\,a} = \vec{r}_1^{\,s} + (1 - \cos\varphi)\left[\vec{n} \cdot \left(\vec{r}_i^{\,a} - \vec{r}_1^{\,s}\right)\right]\vec{n} + \cos\varphi\left(\vec{r}_i^{\,a} - \vec{r}_1^{\,s}\right) + \sin\varphi\,\vec{n} \times \left(\vec{r}_i^{\,a} - \vec{r}_1^{\,s}\right). \tag{15}$$

This formula is used for rotation of the aggregate in all other types of events where rotation of the aggregate is needed. Since the center of mass is moving with the body, its position after the rotation can be calculated with an analogous formula. In order to identify the next event, we determine the pair of contact partners (one sphere of the aggregate, the other from the sediment) which corresponds to the maximal vertical position of the center of mass. In the process of rolling, this event would occur prior to all other potential contacts. When this pair is identified, the whole aggregate is moved to the new position.

For the solution of the system (7)–(9) and its corresponding aggregate position to be a valid future event then two conditions must hold: 1) The center of mass of the aggregate must be lower than in its current position and 2) The new aggregate position should be reachable without center of mass swinging past its lowest point, i.e. the center of mass in the

new position, $\vec{\varrho}_{\rm cm}$, must be on the same side of the plane parallel to $\vec{e}_z$ and $\vec{n}$ and containing the point of rotation, as the current center of mass. The condition 2) can be written as

$$\left[(\vec{r}_{\rm cm}-\vec{r}_1^{\,s})\cdot(\vec{e}_z\times\vec{n})\right]\left[(\vec{\varrho}_{\rm cm}-\vec{r}_1^{\,s})\cdot(\vec{e}_z\times\vec{n})\right]>0. \tag{16}$$

The condition 1) follows from the requirement that the center of mass always performs a descent. If both solutions satisfy conditions 1) and 2), then the solution occurring after smaller angle of aggregate rotation can be identified since its corresponding center of mass is higher. This check is performed before any aggregate position obtained by rotation around an axis is accepted as a valid event. The explicit form of condition 2), Eq. (16), can also be used when the axis is not parallel to the ground.

Once the new contact is established the aggregate has two contacts. Then the aggregate can then either roll on one, newly established, contact or roll on both contacts. If both trajectories are available, then the aggregate will roll on the newly established contact, since for this trajectory the center of mass always descends steeper than for rolling on two contacts.

3.2.3. Event (b) – loss of contact

An aggregate can experience event where it loses contact with s_1, Fig. 4(b) when, due to rotation of the aggregate, sphere a_1 has the same height as s_1. In this rotated position the fixed sphere s_1 is no longer an obstruction and the aggregate falls vertically, following the steepest descent. To calculate this position of a_1, we first find the projection of the center of a_1 onto the axis of rotation, the point $\vec{O}\,'$. The new position where a_1 has the same height as s_1 is

$$\vec{\varrho}_1^{\,a}=\vec{O}\,'+\left|\vec{r}_1^{\,a}-\vec{O}\,'\right|\vec{n}\times\vec{e}_z\,. \tag{17}$$

In this equation it was assumed that $\vec{n}$ is parallel with the horizontal. The cosine and sine of the rotation angle are calculated from the formulas (13)–(14), with index 2 changed to 1. Once the rotation is performed the aggregate falls vertically.

3.2.4. Event (c) – hanging on one contact

The aggregate may rotate at most until its center of mass is exactly below the center of s_1, Fig. 4(c). If in this situation the aggregate sphere a_1 is above the fixed sphere s_1 the aggregate will be stable and hang on this contact. To calculate cosine and sine of the rotation angle needed to reach this event, we consider the position of the center of mass which in the hanging position is

$$\vec{\varrho}_{\rm cm}=\vec{r}_1^{\,s}-\left|\vec{r}_{\rm cm}-\vec{r}_1^{\,s}\right|\vec{e}_z\,. \tag{18}$$

The cosine and sine of the rotation angle can now be found with analogues of (13)–(14), with $\vec{O}\,'=\vec{r}_1^{\,s}$ and by replacing $\vec{r}_2^{\,a}$ with $\vec{r}_{\rm cm}$ and $\vec{\varrho}_2^{\,a}$ with $\vec{\varrho}_{\rm cm}$.

If none of the other events occur, this event is guaranteed to happen, and aggregate will hang on one contact. We note that this type of event is geometrically feasible only for some aggregate shapes, excluding, e.g., convex objects.

3.2.5. Event (d) – collision with the wall

We consider here the case where the aggregate contacts the ground plane, $z=0$, with its constituent sphere a_2. The system of equations to be solved is

$$\left[\vec{\varrho}_2^{\,a}\right]_z=R_2^a \tag{19}$$

$$\left|\vec{\varrho}_2^{\,a}-\vec{r}_1^{\,s}\right|=\left|\vec{r}_2^{\,a}-\vec{r}_1^{\,s}\right| \tag{20}$$

$$\left(\vec{\varrho}_2^{\,a}-\vec{r}_1^{\,s}\right)\cdot\vec{n}=\left(\vec{r}_2^{\,a}-\vec{r}_1^{\,s}\right)\cdot\vec{n} \tag{21}$$

This system is relatively straightforward to solve by elimination since z coordinate of the solution is known, and only one equation contains squares of coordinates. Nevertheless, we solve the system in the similar manner as system (7)–(9), since the procedure is more transparent.

The problem is equivalent to the problem of finding a contact of a point rotating around the axis and contacting the plane $z=R_2^a$. To solve it, we consider the following coordinate system

$$\vec{e}_x'=\vec{n}\times\vec{e}_z\,;\qquad \vec{e}_y'=\vec{n}\times\vec{e}_x'\,;\qquad \vec{e}_z'=\vec{n}\,, \tag{22}$$

whose origin, $\vec{O}\,'$, is at the projection of $\vec{r}_2^{\,a}$ onto the rotation axis. In the x'-y' plane the problem is reduced to an intersection of a circle centered at $\vec{r}^{\,c}=\vec{O}\,'$ and with radius $R^c=\left|\vec{r}_2^{\,a}-\vec{O}\,'\right|$, with a line $y'=\ell$, where

$$\ell\equiv-\frac{\left[\vec{O}\,'\right]_z-R_2^a}{\vec{e}_y'\vec{e}_z} \tag{23}$$

which is now a much simpler problem.

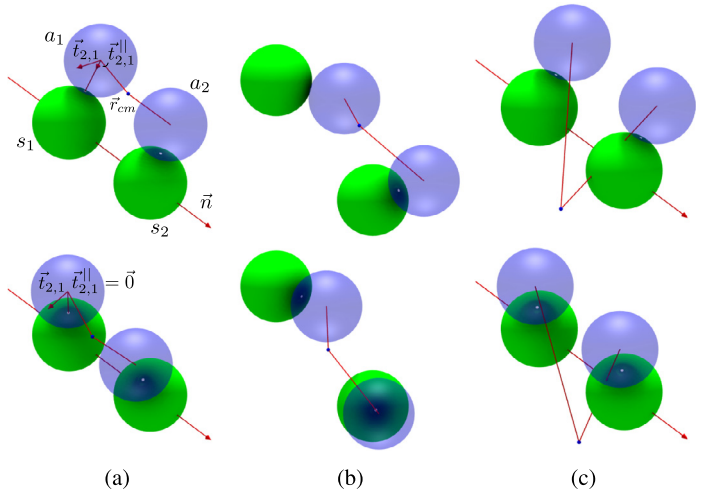

Fig. 6. Prototypical situations for three event types when an aggregate rolls on two contacts. (a) Loss of contact (a_1, s_1). In the final position the component of $\vec{t}_{2,1}$ in direction joining centers of a_1 and s_1, $\vec{t}^{\,||}_{2,1}$, becomes zero and the aggregate can rotate on sphere s_2. (b) The aggregate sphere a_2 attains the same height as s_2, and the aggregate is allowed to fall since a_1 is below s_1. (c) The aggregate rotates around s_1 and s_2 until the center of mass is in the vertical plane through the centers of s_1 and s_2.

3.3. Case (iii) – two contacts

3.3.1. Types of events

When an aggregate is in contact with two spheres of the sediment, 5 different events can result:

(a) the aggregate contacts a third fixed sphere
(b) the aggregate loses one contact
(c) the aggregate loses both contacts
(d) the aggregate rotates until its center of mass is below the rotation axis
(e) the aggregate contacts the wall

Fig. 4 illustrates these cases (except of (a) and (e)) which shall be discussed in detail in the following subsections.

3.3.2. Event (a) – third contact

While rotating on two fixed particles s_1 and s_2, in contact with its two constituent spheres a_1 and a_2 respectively, the aggregate can collide with a fixed sphere. The system of equations for the contact of the aggregate sphere a_3 with the fixed sphere s_3 is obtained from the system (7)–(9) by substituting index 2 by 3, and by having a rotation axis

$$\vec{n} = \frac{\vec{r}^{\,s}_2 - \vec{r}^{\,s}_1}{|\vec{r}^{\,s}_2 - \vec{r}^{\,s}_1|} \tag{24}$$

or equivalently $-\vec{n}$. The obtained system can be solved by the same method as the original system.

After the contact is established, the aggregate has three contacts. Here, the aggregate may either be stable, if further descent is not possible, or continue moving. If it continues moving, then at most three trajectories are available: a) rotation on contacts (a_1, s_1) and (a_3, s_3), b) rotation on contacts (a_2, s_2) and (a_3, s_3) and c) rotation solely on contact (a_3, s_3). Out of available trajectories the one for which the center of mass descends the steepest is chosen.

3.3.3. Event (b) – loss of one contact

During the rotation on two fixed spheres the aggregate may lose one contact, when a trajectory for rotating on one of the spheres is no longer obstructed by the other. Fig. 6(a) shows how such loss of contact occurs for one example. In the initial position, Fig. 6(a) top, the aggregate rotates on two contacts, and therefore trajectories for rotating on each one of the fixed particles are blocked. This condition can be written with the help of the derivative of the position of the aggregate particle a_i with respect to rotation angle φ_j around the fixed particle s_j, assuming rotation in the direction of steepest descent. With the notation $\vec{t}_{j,i} = d\vec{\varrho}^{\,a}_i / d\varphi_j$, the condition that trajectories for rolling on single spheres are blocked is $\vec{t}_{1,2}\left(\vec{r}^{\,a}_2 - \vec{r}^{\,s}_2\right) < 0$ and $\vec{t}_{2,1}\left(\vec{r}^{\,a}_1 - \vec{r}^{\,s}_1\right) < 0$. In Fig. 6(a) top, such condition is satisfied (only at contact (a_1, s_1) vectors are shown). The sphere s_1 no longer obstructs the rotation of the aggregate on contact (a_2, s_2) when

$$\vec{t}_{2,1} \cdot \left(\vec{\varrho}^{\,a}_1 - \vec{r}^{\,s}_1\right) = 0 \tag{25}$$

and if this conditions is satisfied the aggregate can freely rotate around contact (a_2, s_2). We note that as soon as rotation on one contact is available the aggregate will follow this trajectory, since for rotation on one contact the center of mass always descends steeper than for rotation on two contacts. Therefore, to find the aggregate position where it loses contact (a_1, s_1) it is necessary to solve the equation (25), while the aggregate rotates around two contacts. The analogous situation exists in the SDBD algorithm for spheres, however, for aggregates the center of mass does not have to coincide with the center of $\vec{r}_1^{\,a}$ or $\vec{r}_2^{\,a}$.

The equation (25) can be transformed as follows:

$$\vec{t}_{2,1} \cdot \left(\vec{\varrho}_1^{\,a} - \vec{r}_1^{\,s}\right) = 0 \tag{26}$$

$$\left[\vec{n} \times \left(\vec{\varrho}_1^{\,a} - \vec{r}_2^{\,s}\right)\right] \cdot \left(\vec{\varrho}_1^{\,a} - \vec{r}_1^{\,s}\right) = 0 \tag{27}$$

$$\left[\left(\vec{e}_z \times \left(\vec{\varrho}_{\mathrm{cm}} - \vec{r}_2^{\,s}\right)\right) \times \left(\vec{\varrho}_1^{\,a} - \vec{r}_2^{\,s}\right)\right] \cdot \left(\vec{\varrho}_1^{\,a} - \vec{r}_1^{\,s}\right) = 0. \tag{28}$$

The last equation can be further transformed by expanding the triple product

$$\left[\vec{e}_z \cdot \left(\vec{\varrho}_1^{\,a} - \vec{r}_1^{\,s}\right)\right]\left[\left(\vec{\varrho}_1^{\,a} - \vec{r}_2^{\,s}\right) \cdot \left(\vec{\varrho}_{\mathrm{cm}} - \vec{r}_2^{\,s}\right)\right] - \left[\left(\vec{\varrho}_{\mathrm{cm}} - \vec{r}_2^{\,s}\right) \cdot \left(\vec{\varrho}_1^{\,a} - \vec{r}_1^{\,s}\right)\right]\left[\vec{e}_z \cdot \left(\vec{\varrho}_1^{\,a} - \vec{r}_2^{\,s}\right)\right] = 0\,. \tag{29}$$

Defining the constants $A \equiv \left(\vec{\varrho}_1^{\,a} - \vec{r}_2^{\,s}\right) \cdot \left(\vec{\varrho}_{\mathrm{cm}} - \vec{r}_2^{\,s}\right)$ and $B \equiv \left(\vec{\varrho}_{\mathrm{cm}} - \vec{r}_2^{\,s}\right) \cdot \left(\vec{\varrho}_1^{\,a} - \vec{r}_1^{\,s}\right)$, the last equation simplifies:

$$\vec{e}_z\left[(A - B)\,\vec{\varrho}_1^{\,a} + B\vec{r}_2^{\,s} - A\vec{r}_1^{\,s}\right] = 0\,. \tag{30}$$

Equation (30) is an equation of a horizontal plane, for the unknown $\vec{\varrho}_1^{\,a}$. Therefore, this problem can be solved with the same method as the contact of an aggregate sphere with the ground, when the aggregate rotates around an axis. The procedure is also repeated for the contact (a_2, s_2), and valid potential events are added to the event list.

There are special situations for the event type shown in Fig. 6(a) where the condition Eq. (25) is not sufficient do decide whether contact (a_1, s_1) opens such that the aggregate would continue its path by rotating around the other contact (a_2, s_2). This is the case when

$$\frac{d^2}{d\varphi_2^2}\left|\vec{\varrho}_1^{\,a} - \vec{r}_1^{\,s}\right| < 0 \qquad \text{and} \qquad \frac{d}{d\varphi_2}\left|\vec{\varrho}_1^{\,a} - \vec{r}_1^{\,s}\right| = 0 \tag{31}$$

where the latter equation is always true due to Eq. (25). To resolve this situation, we rotate the aggregate by an arbitrarily small angle $\Delta\varphi$ such that Eq. (25) invalidates. If then $\vec{t}_{2,1}\left(\vec{\varrho}_1^{\,a} - \vec{r}_1^{\,s}\right) > 0$, the contact (a_1, s_1) opens, otherwise the aggregate continues rotating with both contacts closed. The concept of the virtual small rotation by $\Delta\varphi$ will be discussed in more detail in Sec. 4.1.

3.3.4. Event (c) – loss of two contacts

While rolling on two contacts the aggregate can lose both contacts at once and start falling directly from rotation on two fixed spheres, Fig. 6(b). In the situation from Fig. 6(b) top, the sphere a_1 is below fixed sphere s_1, and a_2 is slightly above s_2. After rotating until a_2 has the same height as s_2, the aggregate falls vertically, Fig. 6(b) bottom. The problem of finding the position where the aggregate particle a_2 is at the same height as s_2 can be viewed as the problem of contact of a_2 with the horizontal plane $z = z_2^s - R_2^a$, at therefore can be solved by the method already described.

3.3.5. Event (d) – hanging on two contacts

Analogous to the case with one contact, if no collisions take place and there is no loss of contact, the aggregate will rotate until its center of mass is in the vertical plane containing centers of s_1 and s_2, Fig. 6(c). After the rotation the aggregate hangs on its two contacts. To find the position of the center of mass for this situation we first calculate the projection of the center of mass onto the axis of rotation $\vec{n}$, the point $\vec{O}\,'$. The new position of the center of mass is

$$\vec{\varrho}_{\mathrm{cm}} = \vec{O}\,' + \left|\vec{r}_{\mathrm{cm}} - \vec{O}\,'\right| \frac{\vec{n} \times \left(\vec{n} \times \vec{e}_z\right)}{\left|\vec{n} \times \vec{e}_z\right|}, \tag{32}$$

which can now be used to calculate cosine and sine of the rotation angle as for the previous cases.

3.3.6. Event (e) – contact with the ground

The final situation is the contact with the ground while rotating on two contacts. The treatment of this event is identical as for rotation on one contact.

4. Special situations

4.1. Frustrated situations

There are situations for which a certain trajectory which was chosen due to the criterion of steepest descent, become invalidated as soon as the aggregate follows this trajectory, even by an infinitesimal amount. Fig. 7 sketches such a situation

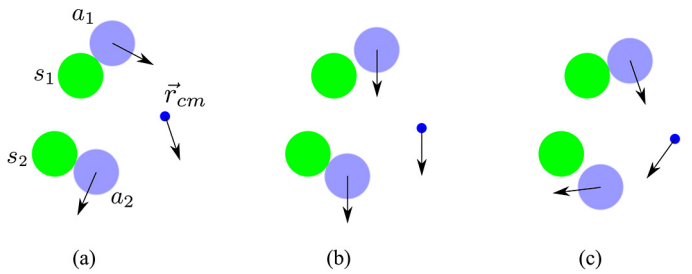

Fig. 7. An example of a frustrated situation. Starting from the configuration (a), the aggregate rolls around the contact (s_2a_2) such that the vertical position of the venter of mass decreases. However, as soon as the aggregate rotated by the tiniest amount, the contact (s_1a_1) opens (b) and the steepest descent would correspond to vertical motion. After performing this vertical motion, the aggregate rotates around (s_1a_1) and a similar situation (c) corresponding to (a) may be assumed.

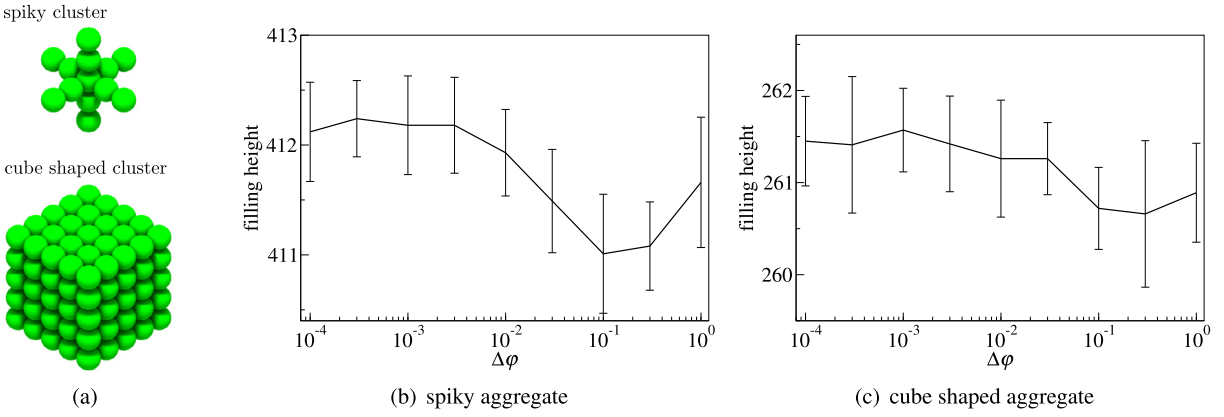

Fig. 8. Influence of $\Delta\varphi$ on the height of a sediment. (a) Two types of aggregates are considered for the analysis. (b), (c) Filling height of 10^4 cube shaped particles and 10^5 spiky particles as functions of $\Delta\varphi$, averaged over 15 independent runs. The error bars show the standard deviation.

which we call *frustrated*, since the steepest descent trajectory violates the requirement of steepest descent as soon as it is followed. Frustrated situations are the result of rolling events around one or two contacts where vertical position of the new contact point (s_na_n) is below the center of s_n, see Fig. 7.

If we would follow the algorithm as described so far, the vertical position of the center of mass would still monotonically decrease, however, we would violate the paradigm of *steepest* descent. Therefore, frustrated situations require special case: in order to assure steepest descent, before performing a rotation around one or two particles we check for a frustrated situation. To this end, we test whether the assumed path of steepest descent remains valid after a rotation of the aggregate by a small angle of typical size $\Delta\varphi \approx 10^{-2}$. If this is not the case, the rotation of the aggregate by $\Delta\varphi$ is added to the list of potential events. This does not mean that the rotation will be performed as there can be another contact corresponding to a yet smaller rotation angle.

As sketched in Fig. 7, depending on the value of $\Delta\varphi$ the sequence (a)–(c) can be repeated several times. The smaller $\Delta\varphi$ the larger is the number of events occurring and, consequently, the needed computer time. On the other hand, $\Delta\varphi$, limits the deviation of the path from the path of steepest descent. Thus, $\Delta\varphi$ compromises between efficiency and precision of the algorithm. To quantify the influence of $\Delta\varphi$, we consider the filling height of a sediment quantified as twice the height of the center of mass of the packing, $2z_{\mathrm{cm}}$, in a box with quadratic bottom of side length 100 particle diameters, Fig. 8. For the test, 10^4 cube shaped particles and 10^5 spiky particles are sedimented, that is a total of 10^6 (cubes) and 1.3×10^6 (spiky particles) constituting spheres. The filling height is averaged over 15 packings. From Fig. 8 we see that the parameter $\Delta\varphi$ has very weak influence on the filling height, causing variations of the mean of less than 0.4%, which drops below the statistical fluctuations. For $\Delta\varphi \lesssim 10^{-2}$ the effect of $\Delta\varphi$ is not noticeable.

Frustrated situations may occur only for concave aggregates and their frequency depends on the shape of the particles. For convex particles such as spheres in the classical algorithm by Visscher and Bolsterli [1] or convex polyhedrons, frustrated situations cannot occur.

4.2. Freezing by infinitely cycling

For certain situations, we observe infinite periodic cycles of contacts which occur in such a way that the vertical position of the center of mass z_{cm} decreases in each cycle but the progress $-\Delta z_{\mathrm{cm}}$ decreases exponentially. We call this scenario *freezing by infinitely cycling* since although the mathematical series for z_{cm} converges to a finite value, this value cannot be

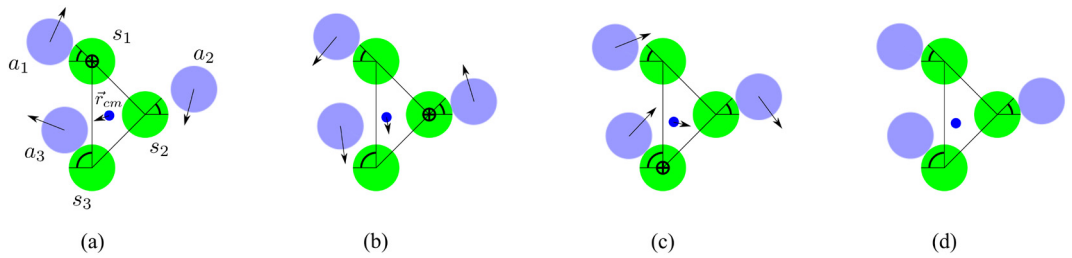

Fig. 9. Sketch of the *freezing by infinitely cycling* scenario. Here the contacts (a_1s_1), (a_2s_2) and (a_3s_3) open and close in cyclic sequence. The vertical position of the center of mass decreases with each cycle but the progress, $-\Delta z_{\rm cm}$, corresponding to one cycle decreases exponentially. (a)–(c) Arrows show the direction of motion of relevant points. Circles with crosses show current rotation points. If contacts are within the arc segments and the x coordinate of the center of mass is to the right of centers of s_1 and s_3 and to the left of s_2, the particle will move towards the fixed point. After situation (c) the particle moves to close the gap (a_1s_1), which then results in the same situation as (a), albeit with smaller gap at s_2. (d) The particle in the fixed point, reached after infinitely many events of type (a)–(c).

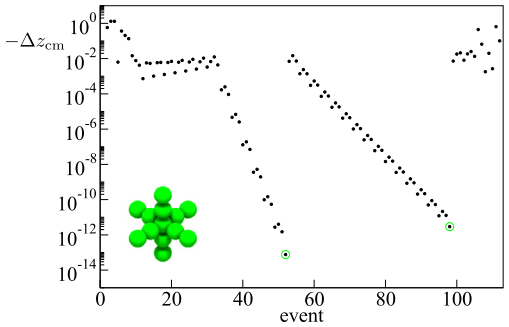

Fig. 10. Decrement of the vertical position of the center of mass, $-\Delta z_{\rm cm}$, over the event number for the deposition of a spiky particle shown as an inset on a sediment created of particles of the same type. To prevent freezing, the sequence is interrupted when $-\Delta z_{\rm cm}$ drops below a threshold. Those events are marked by a green symbol. (For interpretation of the references to color in this figure legend, the reader is referred to the web version of this article.)

achieved by an algorithms since it corresponds to an infinite number of steps. Fig. 9 sketches this scenario for the case of a two-dimensional arrangement, for simpler representation. Starting from Fig. 9(a), with contacts (a_1s_1) and (a_3s_3) closed and (a_2s_2) open. The position is unstable, thus, the particle rolls in (a_1s_1) by opening (a_3s_3) until (a_2s_2) closes, see Fig. 9(b). Now the aggregate rolls in (a_2s_2) by opening (a_1s_1) until (a_3s_3) closes, Fig. 9(c). Thus, all three situations, Fig. 9(a)–(c) are unstable and the procedure repeats *ad infinitum*. In the limes of infinite number of cycles, the system eventually assumes a fixed point where all three contacts are closed, see Fig. 9(d). For two-dimensional problems, infinite cycling converges always to a fixed point which represents a stable local minimum. In contrast, for three-dimensional problems, the fixed point may be unstable, that is, the steepest descent would not terminate when (after an infinite number of steps) the fixed point is reached.

The phenomenon resembles the *inelastic collapse* of an inelastic particle bouncing repeatedly off the ground: Assuming a constant coefficient of restitution, the particle will come to rest after finite (real) time by performing an infinite number of collisions which makes an event-driven algorithm freeze [49] (see [50,51,28,52] how to overcome the inelastic collapse). A detailed mathematical description of the *freezing by infinitely cycling* phenomenon and its relation to the inelastic collapse is given in [53]. Obviously, similar to the inelastic collapse, infinitely cycling does not allow the algorithm to proceed beyond the freezing time. Therefore, we need a way to overcome this situation.

Fig. 10 shows the decrement of the vertical position of the center of mass, $-\Delta z_{\rm cm}$, over a short interval of event numbers. Here we deposited a spiky particle (Fig. 8(a)) on a sediment created of particles of the same type. We observe three different types of behavior: (i) in the intervals of event number $(0, 10)$ and $(100, 110)$ the decrements are irregular and of typical size $-\Delta z_{\rm cm} \approx 0.1 \ldots 1$. (ii) At event number 10 the aggregate enters a frustrated situation and leaves this regime at event number 35. Here the decrements reveal a regular structure of due to cycling as described in Sec. 4.1. In this regime the decrements are slightly smaller than in regime (i), $-\Delta z_{\rm cm} \approx 0.01$. (iii) At event number 35 the system enters the cycling regime where the decrement $-\Delta z_{\rm cm}$ decreases exponentially with progressing event number, which would ultimately lead to freezing if no action is taken to interrupt the cycling. In this regime, a regular structure of period 3 becomes apparent due to the periodic cycling between 3 contacts. For a full description of the regime see [53]. Here we interrupt the cycling at event 52, indicated by the green symbol. The mechanism to interrupt the cycling will be described below. From there, the system immediately transits into another cycling scenario. The second cycling regime is terminated at event number 99. After that, the sedimentation of the aggregate continues by disordered rolling and falling steps, indicated by a decrement scattered in the interval $-\Delta z_{\rm cm} \approx 0.1 \ldots 1$.

When the steepest descent once enters the cycling mode the algorithm inevitably freezes, that is, $-\Delta z_{\mathrm{cm}}$ decreases exponentially, only limited by the machine precision. Therefore, we need a criterion to first identify whether the process is in cycling mode and second to interrupt cycling in order to avoid freezing. A criterion can be derived from the exponential decay in combination with the cycle period 3: Cycling in the interval of event number $(k-n;k)$ implies

$$\frac{\Delta z_{\mathrm{cm}}^{(k)}}{\Delta z_{\mathrm{cm}}^{(k-3)}} = \frac{\Delta z_{\mathrm{cm}}^{(k-1)}}{\Delta z_{\mathrm{cm}}^{(k-4)}} = \frac{\Delta z_{\mathrm{cm}}^{(k-2)}}{\Delta z_{\mathrm{cm}}^{(k-5)}} = \cdots = \frac{\Delta z_{\mathrm{cm}}^{(k-n)}}{\Delta z_{\mathrm{cm}}^{(k-(n+3))}} \tag{33}$$

where $\Delta z_{\mathrm{cm}}^{(m)}$ stands for the decrement of the vertical position of the center of mass in step m. From Eq. (33) we can derive a criterion to decide whether the system is in cycling mode at step k,

$$\frac{\Delta z_{\mathrm{cm}}^{(k)}}{\Delta z_{\mathrm{cm}}^{(k-1)}}\frac{\Delta z_{\mathrm{cm}}^{(k-4)}}{\Delta z_{\mathrm{cm}}^{(k-3)}} < 1+\varepsilon\,; \qquad \frac{\Delta z_{\mathrm{cm}}^{(k-1)}}{\Delta z_{\mathrm{cm}}^{(k-2)}}\frac{\Delta z_{\mathrm{cm}}^{(k-5)}}{\Delta z_{\mathrm{cm}}^{(k-4)}} < 1+\varepsilon\,; \ldots \qquad \frac{\Delta z_{\mathrm{cm}}^{(k-n+1)}}{\Delta z_{\mathrm{cm}}^{(k-n)}}\frac{\Delta z_{\mathrm{cm}}^{(k-n-3)}}{\Delta z_{\mathrm{cm}}^{(k-n-2)}} < 1+\varepsilon \tag{34}$$

for appropriately chosen n and ε, e.g. $(n,\,\varepsilon) = \left(4,\,10^{-3}\right)$. The value of n must not be chosen too large to assure that the increment $|\Delta z_{\mathrm{cm}}|$ is always much larger than the machine precision. If the criteria Eq. (34) are fulfilled, that is, the system approaches a fixed point exponentially, we *declare* the contacts involved in the cycling closed and continue with the next step of the steepest descent path. In practical applications, the remaining clearance of those contacts $\left(a_i, s_j\right)$ was always much smaller than the particle radius, typically $\left|\vec{r}_i^{\,a} - \vec{r}_j^{\,s}\right| - R_i - R_j \ll 10^{-8}$ such that this procedure does not affect the properties of the sediment. A dependence on n and ε was not noticeable in these cases.

4.3. Simultaneous events

In the description so far, it was assumed that not more than one contact is established due to a single event which is true in the vast majority of all events. However, for instance due to finite precision of the calculations, it may happen that two or more contacts are established simultaneously, that is, two (or more) contacts (ij) and (kl) correspond to the same numerical value of smallest falling height $\Delta_{ij}^z = \Delta_{kl}^z = \ldots$ (see Eq. (2)) or rotation angle φ. Similarly, more than one contact may open at the same value of φ. In the algorithm, we can chose the sequence of simultaneously occurring events arbitrarily since any sequence would result in the same configuration of particles. Practically, one of them, e.g. (ij) corresponding to Δ_{ij}^z, would be computed first and the subsequent events will be performed immediately thereafter, e.g. (kl) at $\Delta_{kl}^z = 0$. Simultaneous rotations are handled in the same way, that is, subsequent rotations correspond to $\varphi = 0$. We wish to note that simultaneous events in combination with numerical errors may lead to artefacts which may eventually result in macroscopic interpenetration of particles, that is, invalid states. A convenient way to avoid such artefacts is provided by the concept of *logical states* [54].

5. Discussion and runtime analysis

The described algorithm is tested for two examples of depositions using aggregates of the types shown in Fig. 8 on a horizontal quadratic bottom plate in the $x-y$ plane. Periodic boundary conditions are used for the lateral boundaries. In test (i) we deposit spiky aggregates characterized by the number of spheres, L, along any of the axes, while in test (ii) we use cube like aggregates where L stands for the number of sphere on any of the edges. For the sample pictures shown in Fig. 8(a), $L = 5$. The aggregates are released from randomly chosen points above the bottom plate in randomly chosen angular orientation such that the sediments develop disordered structures, see Fig. 11.

To estimate the efficiency, we computed sediments of 2×10^4 (case i) and 10^4 (case ii) aggregates with $L = 1,\ldots,9$ on a bottom of size 100×100 and measured the time, where the first half of particles was disregarded, in order to provide a disordered bed and to eliminate startup effects. For both types of aggregates, $L = 1$ corresponds to single spheres. In general, spiky particles consist of $3L-2$ spheres and cube-like particles of $6L^2-12L+8$ spheres. Fig. 12 shows the efficiency of the algorithm measured in number of aggregate spheres, ΔN added to the system per unit time Δt; $\Delta\varphi = 0.01$ was chosen (see Sec. 4.1).

We find that the computer time measured in deposited spheres per unit time depends weakly on the size of the aggregates: varying the size of the aggregates by almost 300 (number of constituent spheres) the efficiency varies by a factor less than 2. Therefore, the efficiency of the sedimentation of aggregates composed of linear and/or planar structures may be estimated from the number of spheres it contains, with a fair degree of accuracy.

For the sake of clear presentation, in this paper we considered aggregates built from relatively few monodisperse spheres, however, since there are no restrictions regarding the relative positions of the spheres constituting the aggregate, much more complex shapes are possible, see Fig. 1(e)–(h). Fig. 13 shows examples of heap-like sediments of complex shaped aggregates without lateral boundaries. Fig. 14 shows sediments of complex aggregates with periodic boundary conditions in x and y-direction.

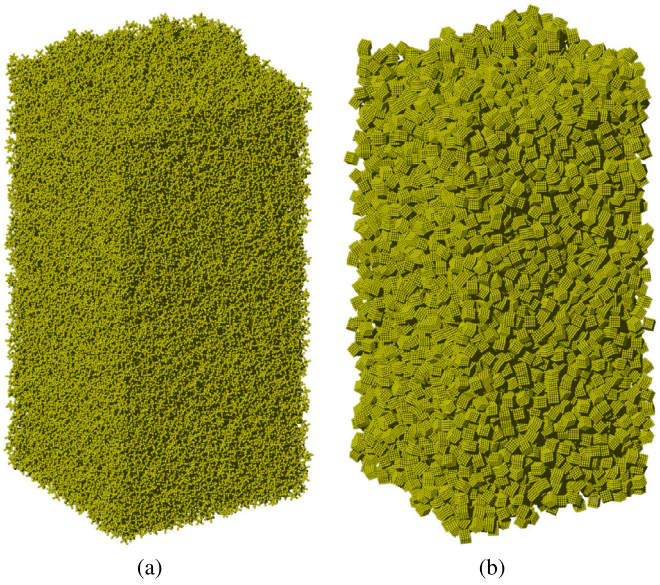

Fig. 11. Sediments of aggregates of the type shown in Fig. 8(a) on a bottom plate of width 200×200 sphere radii. Left: sediment of 5×10^4 spiky aggregates; right: sediment of 8×10^3 cubes-shaped aggregates. $L = 5$ for both particle types.

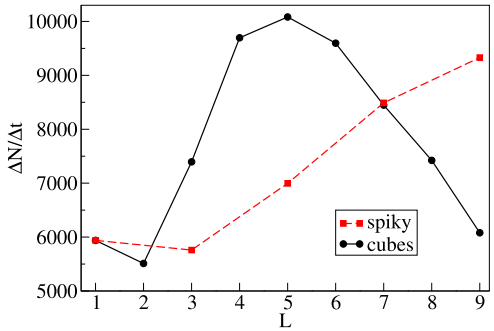

Fig. 12. Efficiency of the algorithm. The picture shows the number of aggregate spheres added to the sediment in unit time. For the estimate we used an Intel Xeon Processor E5-2690 and the vertical axis shows the result for $\Delta t = 1\,\mathrm{s}$.

6. Conclusion

We have developed an event-driven algorithm for the simulation of steepest descent ballistic deposition of complex shaped particles. The constituent polydisperse spheres of the aggregates may be arranged rigidly in overlapping or non-overlapping configuration which allows to describe a variety of shapes, including concave shapes. Our algorithm extends previously described algorithms for the sedimentation of spheres, e.g. [1,30–33], or particles of other simple shapes, e.g. [47,48].

The non-convex shape of aggregates leads to a number of complications, not present in simulations of the sedimentation of convex objects. In particular, we are faced with four situations that cannot appear for convex particles: (i) hanging of the aggregate on one and two contacts; (ii) simultaneous loss of both contacts while rolling; (iii) frustrated situations where a steepest path trajectory in invalidated by even an infinitesimal motion of the aggregate; (iv) freezing by infinite cycling where decrement of the vertical position of the center of mass decays exponentially with the event number.

To overcome these complications, we introduced two parameters, $\Delta\varphi$ and ε. It was checked that $\Delta\varphi$ has a very weak influence on the filling height of the sediments, which changes by less than 0.5% when the parameter is varied over four orders of magnitude. The influence of the other parameter, ε, on the achieved packing was not noticeable in comparison with the statistical noise. The efficiency of the algorithm was investigated for two examples of aggregate shape, one spiky grain type and a compact cube-like type. For both cases we found a weak dependence of the efficiency, measured in total number of sedimented spheres per unit of time, on the size of the aggregates. The described algorithm was successfully applied to the simulation of fractal sediments of nano-particles [10].

By varying the condition for the final position of the aggregate, the algorithm can be extended to the simulation of adhesive particles as well as to systems where the aggregate is subject to fluctuations, e.g. due to thermal fluctuations.

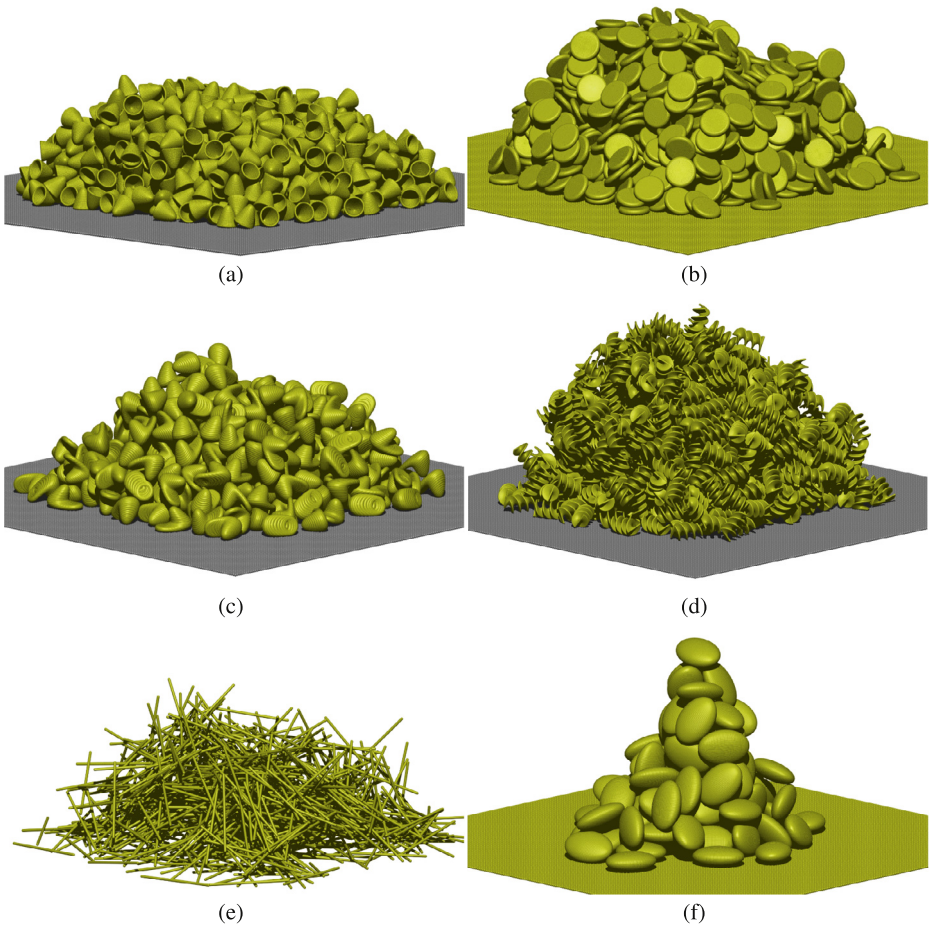

Fig. 13. Examples of heap-like sediments built from complex shaped particles as shown in Fig. 1(e)–(f).

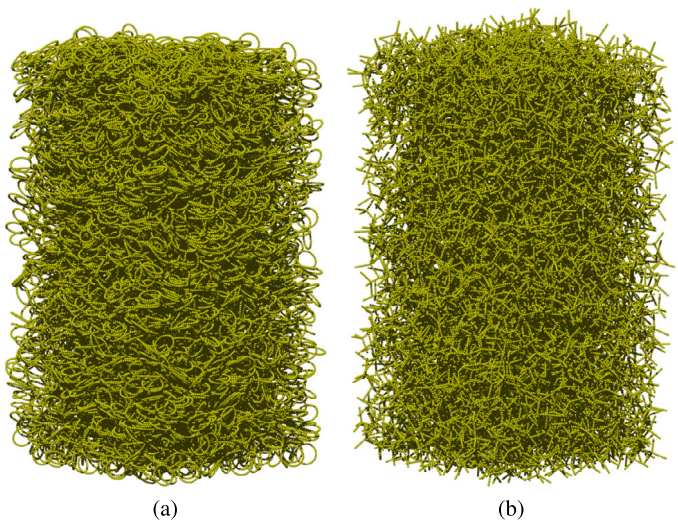

Fig. 14. Examples of sediments of sediments built from rings (Fig. 1(b)) and tripods (Fig. 1(c)) with periodic boundary conditions in both lateral directions.

Acknowledgements

We thank Arno Formella, Patric Müller and Severin Strobl for discussion. We acknowledge the German Research Foundation (DFG) for funding through grant PO 472/22 and through the Cluster of Excellence "Engineering of Advanced Materials" (EXC 315). We gratefully acknowledge the computing time granted by the John von Neumann Institute for Computing (NIC) and provided on the supercomputer JUROPA at Jülich Supercomputing Centre (JSC).

References

[1] W.M. Visscher, M. Bolsterli, Random packing of equal and unequal spheres in two and three dimensions, Nature 239 (1972) 504–507.
[2] L.M. Schwartz, D.J. Wilkinson, M. Bolsterli, P. Hammond, Particle filtration in consolidated granular systems, Phys. Rev. B 47 (1993) 4953.
[3] R. Jullien, P. Meakin, A mechanism for particle size segregation in three dimensions, Nature 344 (1990) 425–427.
[4] R. Jullien, P. Meakin, A. Pavlovitch, Three-dimensional model for particle-size segregation by shaking, Phys. Rev. Lett. 69 (1992) 640–643.
[5] G. Baumann, I.M. Jánosi, D.E. Wolf, Particle trajectories and segregation in a two-dimensional rotating drum, Europhys. Lett. 27 (1994) 203–208.
[6] A. Pavlovitch, R. Jullien, P. Meakin, Geometrical properties of a random packing of hard spheres, Physica A 176 (1991) 206–219.
[7] A. Higgins, Hard sphere packing on an inclined plane, J. Phys. A 29 (1996) 2373–2377.
[8] N. Topic, J.A.C. Gallas, T. Pöschel, Nonuniformities in the angle of repose and packing fraction of large heaps of particles, Phys. Rev. Lett. 109 (2012) 128001.
[9] T. Schwager, D.E. Wolf, T. Pöschel, Fractal substructure of a nanopowder, Phys. Rev. Lett. 100 (2008) 218002.
[10] N. Topic, A. Weuster, T. Pöschel, D.E. Wolf, Structure of a three-dimensional nano-powder subjected to repeated fragmentation and sedimentation, New J. Phys. 17 (2015) 013024.
[11] D. Weaire, T. Aste, The Pursuit of Perfect Packing, 2nd edition, CRC Press, Boca Raton, 2008.
[12] C. Zong, Sphere Packings, Springer, Berlin, 1999.
[13] J. Picka, Statistical inference for disordered sphere packings, Stat. Surv. 6 (2012) 74–112.
[14] A. Benabbou, H. Borouchaki, P. Laug, J. Lu, Geometrical modeling of granular structures in two and three dimensions. Application to nanostructures, Int. J. Numer. Methods Eng. 80 (2009) 425–454.
[15] A.G. Dixon, M. Nijemeisland, E.H. Stitt, Packed tubular reactor modeling and catalyst design using computational fluid dynamics, in: G.B. Marin (Ed.), Adv. Chem. Eng., vol. 31, Academic Press, Waltham, 2006, pp. 307–390.
[16] B.J. Buchhalter, R.M. Bradley, Orientational order in random packings of ellipses, Phys. Rev. A 46 (1992) 3046.
[17] R.M. Baram, P.G. Lind, Deposition of general ellipsoidal particles, Phys. Rev. E 85 (2012) 041301.
[18] C.R.A. Abreu, F.W. Tavares, M. Castier, Influence of particle shape on the packing and on the segregation of spherocylinders via Monte Carlo simulations, Powder Technol. 134 (2003) 167–180.
[19] S.R. Williams, A.P. Philipse, Random packings of spheres and spherocylinders simulated by mechanical contraction, Phys. Rev. E 67 (2003) 051301.
[20] H.J. Tillemans, H.J. Herrmann, Simulating deformations of granular solids under shear, Physica A 217 (1995) 261–288.
[21] T. Pöschel, V. Buchholtz, Molecular dynamics of arbitrarily shaped granular particles, J. Phys. I 5 (1995) 1431–1455.
[22] J. Henzie, M. Grünwald, A. Widmer-Cooper, P.L. Geissler, P. Yang, Self-assembly of uniform polyhedral silver nanocrystals into densest packings and exotic superlattices, Nat. Mater. 11 (2011) 131–137.
[23] X. Jia, R.A. Williams, A packing algorithm for particles of arbitrary shapes, Powder Technol. 120 (2001) 175–186.
[24] J.A.C. Gallas, S. Sokolowski, Grain non-sphericity effects on the angle of repose of granular material, Int. J. Mod. Phys. B 7 (1993) 2037–2046.
[25] V. Buchholtz, T. Pöschel, Numerical investigations of the evolution of sandpiles, Physica A 202 (1994) 390–401.
[26] J. Zhao, S. Li, P. Lu, L. Meng, T. Li, H. Zhu, Shape influences on the packing density of frustums, Powder Technol. 214 (2011) 500–505.
[27] G.T. Nolan, P.E. Kavanagh, Random packing of nonspherical particles, Powder Technol. 84 (1995) 199–205.
[28] T. Pöschel, T. Schwager, Computational Granular Dynamics: Models and Algorithms, Springer, Berlin, Heidelberg, New York, 2005.
[29] W. Soppe, Computer simulation of random packings of hard spheres, Powder Technol. 62 (2) (1990) 189–197.
[30] M.J. Vold, The sediment volume in dilute dispersions of spherical particles, J. Phys. Chem. 64 (1960) 1616.
[31] W.S. Jodrey, E.M. Tory, Simulation of random packing of spheres, Simulation 32 (1979) 1–12.
[32] R. Jullien, P. Meakin, Simple three-dimensional models for ballistic deposition with restructuring, Europhys. Lett. 4 (1987) 1385–1390.
[33] K. Hitti, M. Bernacki, Optimized dropping and rolling (ODR) method for packing of poly-disperse spheres, Appl. Math. Model. 37 (2013) 5715–5722.
[34] E.M. Tory, B.H. Church, M.K. Tam, M. Ratner, Simulated random packing of equal spheres, Can. J. Chem. Eng. 51 (1973) 484–493.
[35] A. Bertei, J. Mertens, C. Nicolella, Electrochemical simulation of planar solid oxide fuel cells with detailed microstructural modeling, Electrochimica 146 (2014) 151–163.
[36] P.M. Nanikashvili, A.V. Butenko, S.R. Liber, D. Zitoun, E. Sloutskin, Denser fluids of charge-stabilized colloids form denser sediments, Soft Matter 10 (2014) 4913.
[37] Y.H. Li, W. Ji, A collective dynamics-based method for initial pebble packing in pebble flow simulations, Nucl. Eng. Des. 250 (2012) 229–236.
[38] D.V. Louzguine-Luzgin, A.R. Yavari, G. Vaughan, A. Inoue, Clustered crystalline structures as glassy phase approximants, Intermetallics 17 (2009) 477–480.
[39] J.H. Zhou, Y.W. Zhang, J.K. Chen, Numerical simulation of random packing of spherical particles for powder-based additive manufacturing, J. Manuf. Sci. Eng. ASME 131 (2009) 031004.
[40] I. Kursun, Determination of mineral processing induced environmental impacts, Asian J. Chem. 18 (2006) 2376–2384.
[41] S.C. Kweon, E. Ramer, A.L. Robinson, Measurement and simulation of ash deposit microstructure, Energy Fuels 17 (2003) 1311–1323.
[42] M. Tassopoulos, J.A. O'Brien, D.E. Rosner, Simulation of mechanism/deposit microstructure relationships in particle deposition, AIChE J. 35 (1989) 967–980.
[43] N.D. Aparicio, A.C.F. Cocks, On the representation of random packings of spheres for sintering simulations, Acta Metall. Mater. 43 (10) (1995) 3873–3884.
[44] W. Ku, O.J. Gregory, H.M. Jennings, Computer simulation of the microstructure developed in reaction-sintered silicon nitride ceramics, J. Am. Ceram. Soc. 73 (2005) 286–296.
[45] C.C. Chueh, A. Bertei, J.G. Pharoah, C. Nicolella, Effective conductivity in random porous media with convex and non-convex porosity, Int. J. Heat Mass Transf. 71 (2014) 183–188.
[46] S. Gao, J.N. Meegoda, L. Hu, Two methods for pore network of porous media, Int. J. Numer. Anal. Methods Geomech. 36 (2012) 1954–1970.
[47] D. Coelho, J.F. Thovert, P.M. Adler, Geometrical and transport properties of random packings of spheres and aspherical particles, Phys. Rev. E 55 (1997) 1959–1978.
[48] M.J. Vold, Sediment volume and structure in dispersions of anisometric particles, J. Phys. Chem. 63 (1959) 1608–1612.

[49] M.N. Bannerman, S. Strobl, A. Formella, T. Pöschel, Stable algorithm for event detection in event-driven particle dynamics, Comp. Part. Mech. 1 (2014) 191–198.
[50] P. Deltour, J.L. Barrat, Quantitative study of a freely cooling granular medium, J. Phys. I 7 (1997) 137–151.
[51] S. Luding, S. McNamara, How to handle the inelastic collapse of a dissipative hard-sphere gas with the tc model, Granul. Matter 1 (1998) 113–128.
[52] R. Reichardt, W. Wiechert, Event driven algorithms applied to a high energy ball mill simulation, Granul. Matter 9 (2007) 251–266.
[53] N. Topic, T. Pöschel, Inelastic collapse of perfectly inelastic particles, submitted for publication, http://msssrv08.mss.uni-erlangen.de/content/uploads/infinite-collision-sequence.pdf.
[54] S. Strobl, M. Bannerman, T. Pöschel, Stable algorithm for event detection in event-driven particle dynamics: Logical states, Comp. Part. Mech. (2016), in press.